HHS Public Access

Author manuscript

Brain Res. Author manuscript; available in PMC 2017 October 01.

Published in final edited form as:

Brain Res. 2016 October 1; 1648(Pt A): 81–89. doi:10.1016/j.brainres.2016.06.042.

Electrophysiological properties of lumbosacral primary afferent neurons innervating urothelial and non-urothelial layers of mouse urinary bladder

Hirosato Kanda, **Buffie J. Clodfelder-Miller**, **Jianguo G. Gu**, **Timothy J. Ness**, and **Jennifer J. DeBerry**[*]

Department of Anesthesiology and Perioperative Medicine, University of Alabama at Birmingham, Birmingham, AL

Abstract

Pelvic nerve (PN) bladder primary afferent neurons were retrogradely labeled by intraparenchymal (IPar) microinjection of fluorescent tracer or intravesical (IVes) infusion of tracer into the bladder lumen. IPar and IVes techniques labeled two distinct populations of PN bladder neurons differentiated on the basis of dorsal root ganglion (DRG) soma labeling, dye distribution within the bladder, and intrinsic electrophysiological properties. IPar (Fast blue)- and IVes (DiI)-labeled neurons accounted for 91.5% (378.3 ± 32.3) and 8% (33.0 ± 26.0) of all labeled neurons, respectively ($p<0.01$), with only 2.0 ± 1.2 neurons labeled by both techniques. When dyes were switched, IPar (DiI)- and IVes (Fast blue) labeled neurons accounted for 77.6% (103.0 ± 25.8) and 22.4% (29.8 ± 10.5), respectively ($P<0.05$), with 6.0 ± 1.5 double-labeled neurons. Following IPar labeling, DiI was distributed throughout non-urothelial layers of the bladder. In contrast, dye was contained within the urothelium and occasionally the submucosa after IVes labeling. Electrophysiological properties of DiI-labeled IPar and IVes DRG neurons were characterized by whole-mount, *in situ* patch-clamp recordings. IPar- and IVes-labeled neurons differed significantly with respect to rheobase, input resistance, membrane capacitance, amplitude of inactivating and sustained K^+ currents, and rebound action potential firing, suggesting that the IVes population is more excitable. This study is the first to demonstrate that IVes labeling is a minimally invasive approach for retrograde labeling of PN bladder afferent neurons, to selectively identify urothelial versus non-urothelial bladder DRG neurons, and to elucidate electrophysiological properties of urothelial and non-urothelial afferents in an intact DRG soma preparation.

Keywords

primary afferent; urinary bladder; urothelium

[*]Correspondence: Jennifer J. DeBerry, PhD University of Alabama at Birmingham Department of Anesthesiology and Perioperative Medicine BMR2-202 901 19th Street South Birmingham, AL 35205. Phone: 205-934-4668; Fax: 205-934-7437. jenniferdeberry@uabmc.edu.

1. Introduction

The urinary bladder stores and evacuates urine via complex reflexes involving coordination between the efferent and afferent branches of the peripheral nervous system. Intravesical pressure during bladder filling is encoded by in-series, low threshold mechanosensitive bladder afferents with receptive fields in the bladder wall that convey information along the pelvic nerve (PN) [1]. Sensitization of these afferents, along with activity in and/or acquisition of mechanosensitivity by other types of afferents, is thought to contribute to bladder hypersensitivity associated with various pathological conditions (e.g., overactive bladder, interstitial cystitis/painful bladder syndrome; see [2]).

Four functionally distinct classes of mechanosensitive PN bladder afferents have been characterized in mouse based upon extracellular recordings of compound action potential firing patterns in response to mechanical stimuli applied to the bladder [3]. All PN bladder afferents responded to blunt probing of their receptive field and were distinguished by their sensitivity to fine urothelial stroking and stretch. Functional classes were described in terms of their putative terminal ending distribution pattern as muscular, urothelial, muscular/mucosal, and serosal [3, 4]. Muscular afferents responded to stretch, urothelial afferents responded to fine stroking, muscular/urothelial fibers responded to both urothelial stroking and graded intensities of bladder stretch, and serosal afferents responded only to probing of their receptive field. Although mechanical stimuli were directed at specific tissue layers, the actual location within the bladder wall of the afferent endings in each class was not determined. Furthermore, extracellular recordings provide little information on the ion channel basis that regulates the intrinsic membrane excitability of afferent neurons. Such mechanisms have been the focus of various other studies that used whole cell patch-clamp recordings of bladder afferent neurons from rat and mouse following acute dissociation or growth in culture conditions [5-19]. A disadvantage of these techniques is that the electrophysiological properties of many neurons may be significantly altered by dissociation, or may vary based on culture medium. The electrophysiological properties of intact bladder afferent neurons have not been reported, presumably because of the technical difficulty associated with performing patch-clamp recordings in intact DRG soma preparation.

To begin to address some of the aforementioned issues, the present study utilized two strategies to retrogradely label bladder primary afferent neurons within lumbosacral dorsal root ganglia (DRG), where the cell bodies of PN afferents are located. Bladder neurons were labeled either by intraparynchemal (IPar) injection or intravesical (IVes) infusion of fluorescent dye into the bladder, and were anatomically differentiated on the basis of dye distribution in the bladder wall and neuron soma labeling in the DRG. For simplicity, we will refer to neurons labeled by IPar injection as “non-urothelial” and the periurothelial afferents labeled by IVes infusion as “urothelial.” *In situ* patch-clamp recordings from non-urothelial and urothelial bladder afferent neurons were performed using a whole-mount DRG preparation that more closely approximates the *in vivo* condition than previously used methods. The results of these studies indicate that non-urothelial and urothelial subpopulations of bladder-innervating neurons exhibit differences in electrophysiological characteristics that reflect neuronal excitability.

2. Results

2.1 Anatomical properties of urothelial and non-urothelial bladder afferents

In two groups of mice, we determined the number of bladder primary afferent DRG neurons that were retrogradely labeled by IPar injection and IVes infusion of dye (**Figure 1**). There was a profound effect of the route of dye administration on the number of labeled neurons ($P<0.0001$). When Fast blue (FB) was delivered IPar and 1,1'-dioctadecyl-3,3,3',3'-tetramethylindocarbocyanine perchlorate (DiI) was delivered IVes (**Figure 1A-C**), FB-positive neurons accounted for 91.5% (378.3 ± 32.3 neurons per mouse) of labeled L6 neurons, whereas DiI-positive neurons accounted for only 8% (33.0 ± 26.0 neurons per mouse) of labeled L6 neurons ($P<0.01$, n=3; **Figure 1D,E**). The degree of overlap between subsets of labeled neurons was virtually nonexistent, with only 2.0 ± 1.2 neurons per mouse expressing both FB and DiI, corresponding to 6.06% of DiI-positive co-labeled with FB and 0.53% of FB-positive co-labeled with DiI. A similar pattern of labeling was observed with IPar DiI and IVes FB, although the relative proportions of IVes- and double-labeled afferents were greater, and the proportion of IPar-labeled neurons smaller (n=2; **Figure 1F**). Parallel experiments in a third group of mice were done in which IVes DiI was combined with injection of FB into the urethra to determine whether labeling of somatic urethral neurons may have occurred during transurethral delivery of dye for intravesical labeling of bladder neurons. >99% of FB-positive urethral neurons were DiI-negative (n=4).

In all cases, labeled neuron counts were based on a 4 h intravesical dwell time of dye, although a subsequent parametric analysis showed that a 2 h dwell time was as effective (**Figure 2**).

To examine how fluorescent dye was distributed within bladder tissue following dye administration by IPar and IVes techniques, we harvested bladder tissue 1 h, 24 h, or 1 wk following IVes infusion of DiI into the bladder lumen, and 1 wk following IPar microinjection of DiI into the bladder wall. Time- and technique-dependent patterns of DiI distribution were observed. IPar administration of DiI produced a uniform distribution of DiI throughout the bladder smooth muscle, with no spread into the urothelium (**Figure 3A,B**). In contrast, DiI was restricted to the periurothelial region 1 h following IVes infusion (**Figure 2D,E**). Quantitative analysis of integrated density of bladder tissue from IPar- and IVes-labeled mice revealed significant differences in urothelial and non-urothelial fluorescence that was dependent upon technique (**Figure 2C**). The integrated density in IPar-labeled bladder tissue was significantly higher in non-urothelial than in urothelial areas ($P<0.05$), and in IVes-labeled tissue was significantly higher in urothelial areas than non-urothelial areas ($P<0.01$). Within IPar-labeled tissue, non-urothelial labeling was significantly greater than urothelial labeling ($P<0.05$), and the opposite was true for IVes-labeled tissue ($P<0.01$). Anecdotally, diffusion of DiI into the submucosa was observed 24 h following IVes infusion (data not shown), but quantitative analysis of regions that were clearly urothelial versus non-urothelial indicated no diffusion into non-urothelial tissue (**Figure 3F**).

2.2 Electrophysiological properties of urothelial and non-urothelial bladder afferents

A combination of differential interference contrast and epifluorescence illumination was used to identify retrogradely labeled neurons for patch-clamp recordings in whole-mount L6 DRG (**Figure 4A,B**). The success rate in achieving a high quality seal between the recording electrode and membrane of targeted DRG neurons using this preparation is decreased due to the fact that electrodes must penetrate layers of cells, including satellite cells that enwrap the targeted neuron. Thus, to maintain accuracy of electrophysiological parameters, data was collected from neurons with baseline whole-cell currents of ≤50 pA (Vh = −73 mV) that included a total of 10 IPar- and 10 IVes-labeled DRG neurons (3 mice per group). The labeled IPar and IVes neurons had mean diameters of 21.3 ± 0.5 μm (n=10) and 20.7 ± 0.5 μm (n=10), respectively (P=0.86). **Figure 4C** shows typical membrane responses to current injections via patch-clamp recording electrodes into an IPar and IVes neuron. Both types of neurons exhibited inflected somal spikes in the repolarization phase (**Figure 4D**). Neither type of neuron displayed spontaneous activity, nor did they differ in resting membrane potential (**Figure 4E**). However, the rheobase of IPar neurons was 301 ± 50 pA, about 3-fold that of IVes neurons (P<0.001; **Figure 4F**). There was no difference in AP threshold or width (**Figures 4G,H**), and 90% (9/10) of the neurons in each group fired single APs in response to suprathreshold current injection up to 3-10× rheobase (**Figure 4I**). However, 70% (7/10) of IVes neurons, but none of the IPar neurons, exhibited hyperpolarization-induced rebound APs (P<0.01, **Figure 4J**). This may be attributed, at least in part, to the more prominent hyperpolarization-activated “sag” potential in response to hyperpolarizing current injections in IVes neurons (**Figures 4C,K**). Input resistance in IPar neurons was 332.1 ± 32.1 MΩ, ~30% lower than the input resistance of IVes neurons (P<0.05; **Figure 4L**). Membrane capacitance (**Figure 4M**) was 24.5 ± 2.5 and 18.0 ± 1.6 pF in IPar- and IVes-labeled neurons, respectively (P<0.05).

Voltage-activated currents were examined under voltage-clamp configuration. Voltage-activated currents were elicited by voltage steps ranging from −90 to +70 mV in increments of 10 mV and 250 ms duration. As shown in **Figure 5A,B**, two main currents were observed in response to the voltage steps. First, a transient inward current appeared at the beginning of the voltage steps that is primarily due to the activation of voltage-gated Na^+ channels. Second, an outward current due to the activation of inactivating and non-inactivating voltage-gated K^+ channels appeared. When inward currents were estimated with no attempt to isolate them from the sustained outward currents, there was no difference between IPar and IVes neurons (**Figure 5B**). In contrast, voltage-activated outward currents were significantly larger in IPar neurons than in IVes neurons. Specifically, in IPar neurons the peak amplitude of inactivating current was significantly greater in response to voltage steps from −30 to +70 mV (P<0.05; **Figure 5C**), and the amplitude of non-inactivating current, as measured at the end of each voltage step, was significantly greater at voltage steps of −10 to +70 (P<0.05; **Figure 5D**). In addition to the currents observed during voltage steps, both IPar and IVes bladder neurons exhibited M-type voltage-gated K^+ currents (M-currents), measured by tail currents of total K^+ current deactivation. Representative traces from IPar and IVes neurons during deactivation from −20 to −60 mV show similar magnitude of M-currents with mean peak amplitudes of 182.8 ± 20.1 pA and 174.1 ± 19.4 pA, respectively

(n=10/group; **Figures 6A,B**). M-currents quantified over a range of voltage steps did not differ between neuron types (**Figures 6C,D**).

3. Discussion

Direct microinjection of tracer into the urinary bladder parenchyma (i.e., IPar) is the traditional method for retrogradely labeling the cell bodies of bladder-innervating primary afferent neurons. This study is the first to demonstrate that intravesical infusion of tracer into the bladder lumen (i.e., IVes) is another useful approach for retrogradely labeling bladder afferent DRG neurons. However, the most important finding of this study extends beyond proof-of-concept of an alternative labeling strategy; anatomical and electrophysiological data indicate that IVes-labeled neurons represent a subset of bladder afferents distinct from those traditionally labeled by IPar dye injection. We observed virtually no overlap in FB-labeled IPar and DiI-labeled IVes neurons (6 out of 1240 labeled L6 neurons in 3 mice). Bladder histology suggests that DiI-positive, IVes-labeled neurons, which represent 8% of all labeled neurons, are those with peripheral terminal endings located in the urothelium [20-24]. This is supported by evidence from single fiber electrophysiological recordings showing that a comparable proportion (9%) of PN afferents exhibited ‘urothelial’ type mechanical response profiles [3]. The remaining 91% of functionally identified afferents, comprised of muscular (63%), muscular/mucosal (14%), and serosal (14%) subtypes, is equivalent in proportion to FB-positive, IPar-labeled neurons in the present study. The bladder wall contains low-threshold, in-series-coupled mechanosensitive afferents, high threshold mechanosensitive afferents, and mechanically insensitive afferents that acquire mechanosensitivity following sensitization [25-27]. It is possible that urothelial afferents identified via single fiber recordings that do not normally respond to bladder stretch comprise the latter group of ‘silent’ afferents, or a subset of this group. Regardless, those afferents with terminal endings in proximity to the urothelium express ligand-gated receptors for a variety of urothelial-derived mediators that increase afferent signaling [28]. Characterization of the somal properties of this newly identified, IVes-labeled group of afferents during/following organ injury or inflammation may yield new insights for understanding pathological changes in bladder sensation and function.

An important caveat in the present study is that the high degree of specificity of urothelial afferent labeling is dependent upon the use of IVes DiI, as IVes FB labeled a larger, less specific, proportion of afferents and yielded a greater degree of overlap between IPar- and IVes-labeled neurons. It has previously been reported that differences in uptake of FB and DiI *administered in a similar fashion* do not differentially label neuron populations [29], however we observed differences in distribution within the bladder with IVes FB (data not shown). DiI is a lipophilic dye that mainly acts via passive diffusion along membrane surfaces. In our study, DiI was dissolved in DMSO prior to dilution. Compounds with high lipophilicity, such as paclitaxel, have been shown to penetrate the urothelium to a greater degree than other drugs when used in the intravesical treatment of bladder cancer [30]. Further, DMSO has been shown to affect cellular phospholipid membranes by increasing lateral distance between lipid heads, facilitating the entrance of water [31]. In the current study, little to no DiI was detected below the urothelium when delivered intravesically. This

may be due to its drainage into capillaries as it diffuses toward the basal urothelium, as has been indicated for other lipophilic compounds [32].

Previous electrophysiological studies of bladder primary afferents have used dissociated DRG neurons following intraparynchmal retrograde labeling. To the authors' knowledge, the present study is the first to perform patch-clamp recordings of bladder-innervating neurons in whole-mount DRG, a preparation that more closely resembles *in vivo* conditions. The most interesting conclusion from the current studies is drawn from observed differences in several electrophysiological characteristics between non-urothelial (IPar) and urothelial (IVes) bladder neurons that, taken together, indicate higher excitability of urothelial neurons. Urothelial neurons had a significantly lower rheobase relative to non-urothelial neurons, and were more likely to fire rebound action potentials induced by hyperpolarization. Urothelial and non-urothelial neurons also significantly differed with respect to their input resistance, which may partially account for the observed difference in rheobase. The input resistance of a cell is mainly regulated by two-pore-domain "leak" K^+ channels including TREK-1, TREK-2, and TRAAK that are expressed in mouse bladder PN primary afferents [33]. Future experiments are required to determine the relative expression of these K^+ channels in urothelial and non-urothelial neurons.

The electrophysiological profiles of urothelial and non-urothelial afferents also suggest differences in expression of voltage-gated K^+ (Kv) channels. Significantly higher amplitudes of inactivating and non-inactivating K^+ currents were observed in non-urothelial neurons. A-type K^+ currents profoundly regulate sensory neuron excitability [9, 11, 14], and may be mediated by Kv4.3 [34] or by Kv1.4, which is responsible for A-type currents in rat bladder neurons. Both urothelial and non-urothelial neurons exhibited substantial M-currents, mediated by the Kv7 family of channels encoded by KCNQ genes. Kv7 expression in primary afferents has been shown to contribute to neuronal excitability in trigeminal and DRG neurons, including those innervating the bladder [34-37]. Larger M-currents have been shown to be associated with single AP firing pattern in sensory neurons [38]. Consistently, 90% of urothelial and non-urothelial neurons showed single AP firing pattern. It will be the task of future studies to determine whether downregulation of these voltage-gated K^+ channels may account for heightened sensory neuron excitability seen under pathological conditions.

An important consideration is whether and/or how the current findings change the interpretation of multiple published studies that only used IPar labeling techniques, and in which urothelial afferent mechanisms may have been omitted by default. A gross comparison of whole-mount electrophysiological data with data from previously published studies [39] using dissociated, IPar-labeled PN bladder neurons suggests some important differences. In comparison to whole-mount IPar neurons, dissociated IPar bladder neurons had a lower rheobase and higher input resistance. These differences are independent of a difference in capacitance, which was similar between techniques and ranged from 20-45 pF [39]. Multiple recent studies in the somatosensory system have underscored the importance of chemical signaling from 'non-neuronal' cells (e.g., Merkel cells, keratinocytes) to primary afferent neurons [40-42]. Given that urothelial dysfunction appears to be a pathophysiological component of symptom development in interstitial cystitis/painful

bladder syndrome (IC/PBS), IVes or urothelial afferent mechanisms may be of particular importance for the translational relevance of previous labeled neuron studies. A separate technical consideration for future studies employing the IVes labeling technique is whether dissociated neuron cultures will prove to be useful. IVes-labeled neurons were readily identifiable using a whole mount DRG preparation despite constituting only 9% of the total labeled bladder neuron population. It is estimated <10% of spinal afferent DRG neurons innervate the viscera [1, 43-45], with approximately 6% innervating the bladder [46]. The vast majority of neurons comprising a ganglion are lost during dissociation procedures, and retention of such a small proportion of IVes-labeled neurons in a dissociated neuron culture may be challenging.

In summary, intravesical labeling is a novel technique with demonstrated utility for identifying presumed urothelial bladder afferent neurons with unique electrophysiological characteristics from non-urothelial (IPar) afferents. It is the goal of future studies to now determine the functional significance of these characteristics.

4. Experimental Procedure

4.1 Animals

Experiments were performed on female C57Bl/6 mice, 20-25 g in weight (Charles River). Only females were used due to the difficulty in transurethral bladder cannulation of male animals. Mice were housed in standard cages with *ad libitum* access to food and water in the University of Alabama at Birmingham (UAB) Animal Resources Program. All procedures were approved by the UAB Institutional Animal Care and Use Committee and met the standards for humane animal care and use set forth by the Animal Welfare Act and the NIH Guide for the Care and Use of Laboratory Animals.

4.2 Retrograde neuronal labeling

To label the soma of bladder-projecting primary afferent neurons, fluorescent dye was either injected into the bladder parenchyma (intraparynchmal; IPAR) or infused into the bladder lumen (intravesical; IVes) of isoflurane-anesthetized (5% in oxygen induction, 1-2% maintenance) mice. 1,1'-dioctadecyl-3,3,3',3'-tetramethylindocarbocyanine perchlorate (DiI; Molecular Probes) was dissolved at 170 mg/mL in dimethylsulfoxide and diluted 1:10 in 0.9% sterile saline. Fast blue (FB; Polysciences Inc.) was used as a 1% w/v solution in water. For IVes labeling, 60 μL of DiI was delivered via a transurethrally placed 24-gauge angiocatheter and left to dwell in the bladder for four h (except where noted for parametric studies). Bladders were drained and mice returned to their home cages. For IPAR labeling, a laparotomy was performed to expose the bladder and dye was injected via microsyringe (three injections, total volume 10 μL). Abdominal muscles and overlying skin were sutured separately. In one group of mice, IPAR FB labeling preceded IVes DiI labeling by 24 h to determine the degree of overlap between IPAR and IVes neurons.

4.3 Histology

Mice were deeply anesthetized with isoflurane and transcardially perfused with 4% paraformaldehyde. L6 DRG were dissected, post-fixed overnight, then cryoprotected in 30%

sucrose. Ganglia pairs were embedded together, sectioned via cryostat at 10 μm, slide mounted, washed (3 × 5 min in PBS), and coverslipped using 50% glycerol in PBS. Tissue sections were viewed on a Nikon TI80E microscope (Nikon Instruments, Inc.), and photomicrographs were made using NIS-Elements software and saved to computer. Peak excitation/emission for DiI and FB are 549/565 and 360/410, respectively. For double-labeled DRG, photomicrographs were taken at 10× of every other tissue section throughout each ganglion. For parametric studies comparing intravesical DiI exposure times, slide-mounted tissue sections were washed (5 min) in bisbenzimide (1 μl/ml of a 0.2% w/v solution) prior to being coverslipped. Photomicrographs of serial sections throughout each ganglion were taken at 10×, and labeled neurons with a visibly stained nucleus were counted. To determine the location and extent of tracer distribution in bladder tissue, bladders were harvested from a subset of mice following transcardial perfusion with 4% paraformaldehyde at 1 h, 24 h, or one wk following IVes DiI infusion or one wk following IPar DiI injection. Photomicrographs were taken at 10× for quantitative analysis. Using NIH ImageJ, a grid (7000 pixels^2 area per point) was overlaid on bright field images of three non-sequential tissue sections per mouse (n=3/group) in the one wk post-labeling groups using the Analyze plug-in. Five grid boxes of urothelial and five of non-urothelial tissue were chosen by an experimenter blinded to the dye administration condition. Then, the same grid boxes were identified on fluorescence images of the same tissue sections and contrast was adjusted (low end 34, high end 220) to remove background. Integrated density was measured and normalized to pixel area. Data are shown as mean integrated density / pixel area.

4.4 Patch-clamp recordings

One wk after IPar DiI injection or IVes DiI infusion, mice were deeply anesthetized with isoflurane and decapitated. Bilateral L6 DRG were rapidly dissected into cold Leibovitz-15 medium (Mediatech, Inc.) and surface connective tissues were carefully removed. Whole DRG were anchored in a recording chamber mounted on the stage of an Olympus IX50 microscope and submerged in a Krebs solution containing (in mM): 117 NaCl, 3.5 KCl, 2.5 $CaCl_2$, 1.2 $MgCl_2$, 1.2 NaH_2PO_4, 25 $NaHCO_3$, and 11 glucose, with pH 7.3 and 325 mOsm and saturated with 95% O2 and 5% CO2. DRG were exposed to 0.05% dispase II and 0.05% collagenase in the Krebs solution for 3-5 min prior to being washed off in enzyme-free Krebs solution, and then DRG were continuously perfused at 2 ml/min with Krebs solution at room temperature. Retrogradely labeled neurons were first identified under epifluorescence illumination and then viewed using an infrared differential intensity contrast optical system. Whole-cell patch-clamp recordings were performed on randomly selected labeled neurons. Electrodes for patch-clamp recordings were fabricated from thin-wall capillaries using a Flaming/Brown P-97 puller (Sutter Instrument Co.). Recording electrodes had resistances of 6 MΩ when filled with internal solution containing (in mM) 105 K-Gluconate, 35 KCl, 2.4 $MgCl_2$, 0.5 $CaCl_2$, 5 EGTA, 10.0 HEPES, 5.0 Na_2ATP, 0.33 GTP-Tris salt; pH 7.35 (adjusted with Tris-base) and 320 mOsm (adjusted with sucrose). Signals were amplified using an Axopatch 200B amplifier (Axon Instruments) with a low-pass filter set at 2 kHz and digitized at 10 kHz. Data were acquired using pCLAMP10 software (Axon Instruments). Junction potential between bath and electrode solution was calculated to be −13 mV and was corrected for in the data analysis.

After gaining whole-cell access and in voltage-clamp mode, membrane capacitance and input resistance were measured at the beginning of the recording using a seal test with voltage pulses of 5 mV. Unless otherwise indicated, neurons were held at −73 mV (voltage command at −60 mV). To determine voltage-activated currents, whole-cell currents were evoked by a series of voltage steps ranging from −103 to +57 mV in 10 mV increments of 250 ms. Isolation of Na^+ or K^+ currents was not performed in this study. To examine M-currents in bladder DRG neurons, deactivating tail currents were measured following the voltage step of −20 mV as described previously [35].

Resting membrane potential and spontaneous activity were determined upon switching to current-clamp mode. To determine membrane excitability, step current pulses from −100 to +900 pA (20 pA per step, 250 ms duration) were injected into cells through patch-clamp electrodes. Neuronal excitability was characterized by action potential (AP) threshold, rheobase, number of APs evoked in response to depolarizing current injection, and spontaneous activity [47]. Rheobase was defined as the least amount of current required to evoke an AP and AP threshold was defined as the greatest depolarization reached before AP generation. Other passive and active electrophysiological properties were assessed including cell capacitance, input resistance, and AP amplitude, width, and shape.

4.5 Data Analysis

Pooled data are presented as mean ± SEM. The number of IPAR- and IVes-labeled neurons was compared by one-way ANOVA and post-hoc t-tests with Welch's correction for unequal variances where necessary. Parametric analysis of the number of IVes-labeled neurons by dye infusions of varying duration was performed by one-way ANOVA and post-hoc Student's t-tests. Electrophysiological data from IPAR- and IVes-labeled neurons were analyzed using pCLAMP software and Clampfit 10 module (Molecular Devices) and were compared using Student's t-tests. P values <0.05 were considered significant.

Acknowledgements

This work was supported by NIH grants DE023090 and DE018661 (JGG), DK51413 (TJN), and DK101681 (JJD).

References

1. Janig W, Morrison JF. Functional properties of spinal visceral afferents supplying abdominal and pelvic organs, with special emphasis on visceral nociception. Prog Brain Res. 1986; 67:87–114. [PubMed: 3823484]
2. Nickel JC, et al. Continuous intravesical lidocaine treatment for interstitial cystitis/bladder pain syndrome: safety and efficacy of a new drug delivery device. Sci Transl Med. 2012; 4(143): 143ra100.
3. Xu L, Gebhart GF. Characterization of mouse lumbar splanchnic and pelvic nerve urinary bladder mechanosensory afferents. J Neurophysiol. 2008; 99(1):244–53. [PubMed: 18003875]
4. Brierley SM, et al. Splanchnic and pelvic mechanosensory afferents signal different qualities of colonic stimuli in mice. Gastroenterology. 2004; 127(1):166–78. [PubMed: 15236183]
5. Yoshimura N, et al. The involvement of the tetrodotoxin-resistant sodium channel Na(v)1.8 (PN3/SNS) in a rat model of visceral pain. J Neurosci. 2001; 21(21):8690–6. [PubMed: 11606657]
6. Yoshimura N, et al. Histological and electrical properties of rat dorsal root ganglion neurons innervating the lower urinary tract. J Neurosci. 2003; 23(10):4355–61. [PubMed: 12764124]

7. Yoshimura N, De Groat WC. Characterization of voltage-sensitive Na+ and K+ currents recorded from acutely dissociated pelvic ganglion neurons of the adult rat. J Neurophysiol. 1996; 76(4): 2508–21. [PubMed: 8899623]
8. Sculptoreanu A, Yoshimura N, de Groat WC. KW-7158 [(2S)-(+)-3,3,3-trifluoro- 2-hydroxy-2-methyl-N-(5,5,10-trioxo-4,10-dihydrothieno[3,2-c][1]benzothiepin-9- yl)propanamide] enhances A-type K+ currents in neurons of the dorsal root ganglion of the adult rat. J Pharmacol Exp Ther. 2004; 310(1):159–68. [PubMed: 15010502]
9. Takahashi R, et al. Hyperexcitability of bladder afferent neurons associated with reduction of Kv1.4 alpha-subunit in rats with spinal cord injury. J Urol. 2013; 190(6):2296–304. [PubMed: 23896350]
10. Masuda N, et al. Characterization of hyperpolarization-activated current (Ih) in dorsal root ganglion neurons innervating rat urinary bladder. Brain Res. 2006; 1096(1):40–52. [PubMed: 16765328]
11. Hayashi Y, et al. Bladder hyperactivity and increased excitability of bladder afferent neurons associated with reduced expression of Kv1.4 alpha-subunit in rats with cystitis. Am J Physiol Regul Integr Comp Physiol. 2009; 296(5):R1661–70. [PubMed: 19279288]
12. Black JA, et al. Tetrodotoxin-resistant sodium channels Na(v)1.8/SNS and Na(v)1.9/NaN in afferent neurons innervating urinary bladder in control and spinal cord injured rats. Brain Res. 2003; 963(1-2):132–8. [PubMed: 12560118]
13. Waterman SA. Multiple subtypes of voltage-gated calcium channel mediate transmitter release from parasympathetic neurons in the mouse bladder. J Neurosci. 1996; 16(13):4155–61. [PubMed: 8753877]
14. Yunoki T, et al. Differential contribution of Kv4-containing channels to A-type, voltage-gated potassium currents in somatic and visceral dorsal root ganglion neurons. J Neurophysiol. 2014; 112(10):2492–504. [PubMed: 25143545]
15. Yoshimura N, de Groat WC. Plasticity of Na+ channels in afferent neurones innervating rat urinary bladder following spinal cord injury. J Physiol. 1997; 503(Pt 2):269–76. [PubMed: 9306271]
16. Hougaard C, et al. A positive modulator of K Ca 2 and K Ca 3 channels, 4,5-dichloro- 1,3-diethyl-1,3-dihydro-benzoimidazol-2-one (NS4591), inhibits bladder afferent firing in vitro and bladder overactivity in vivo. J Pharmacol Exp Ther. 2009; 328(1):28–39. [PubMed: 18820135]
17. Lei Q, Malykhina AP. Colonic inflammation up-regulates voltage-gated sodium channels in bladder sensory neurons via activation of peripheral transient potential vanilloid 1 receptors. Neurogastroenterol Motil. 2012; 24(6):575–85. e257. [PubMed: 22420642]
18. Malykhina AP, et al. Colonic inflammation increases Na+ currents in bladder sensory neurons. Neuroreport. 2004; 15(17):2601–5. [PubMed: 15570160]
19. Yoshimura N, Seki S, de Groat WC. Nitric oxide modulates Ca(2+) channels in dorsal root ganglion neurons innervating rat urinary bladder. J Neurophysiol. 2001; 86(1):304–11. [PubMed: 11431511]
20. Birder LA, et al. Vanilloid receptor expression suggests a sensory role for urinary bladder epithelial cells. Proc Natl Acad Sci U S A. 2001; 98(23):13396–401. [PubMed: 11606761]
21. Birder LA, et al. Altered urinary bladder function in mice lacking the vanilloid receptor TRPV1. Nat Neurosci. 2002; 5(9):856–60. [PubMed: 12161756]
22. Dickson A, et al. Peptidergic sensory and parasympathetic fiber sprouting in the mucosa of the rat urinary bladder in a chronic model of cyclophosphamide-induced cystitis. Neuroscience. 2006; 141(3):1633–47. [PubMed: 16989017]
23. Jen PY, Dixon JS, Gosling JA. Immunohistochemical localization of neuromarkers and neuropeptides in human fetal and neonatal urinary bladder. Br J Urol. 1995; 75(2):230–5. [PubMed: 7531592]
24. Kunze E, et al. Transitional cell carcinomas and nonurothelial carcinomas of the urinary bladder differ in the promoter methylation status of the caveolin-1, hDAB2IP and p53 genes, but not in the global methylation of Alu elements. Int J Mol Med. 2006; 17(1):3–13. [PubMed: 16328005]
25. Habler HJ, Janig W, Koltzenburg M. Activation of unmyelinated afferent fibres by mechanical stimuli and inflammation of the urinary bladder in the cat. J Physiol. 1990; 425:545–62. [PubMed: 2213588]

26. Rong W, Spyer KM, Burnstock G. Activation and sensitisation of low and high threshold afferent fibres mediated by P2X receptors in the mouse urinary bladder. J Physiol. 2002; 541(Pt 2):591–600. [PubMed: 12042363]
27. Wen J, Morrison JF. The effects of high urinary potassium concentration on pelvic nerve mechanoreceptors and 'silent' afferents from the rat bladder. Adv Exp Med Biol. 1995; 385:237–9. [PubMed: 8571836]
28. Kanai A, et al. Researching bladder afferents-determining the effects of beta(3) - adrenergic receptor agonists and botulinum toxin type-A. Neurourol Urodyn. 2011; 30(5):684–91. [PubMed: 21661014]
29. Choi D, Li D, Raisman G. Fluorescent retrograde neuronal tracers that label the rat facial nucleus: a comparison of Fast Blue, Fluoro-ruby, Fluoro-emerald, Fluoro-Gold and DiI. J Neurosci Methods. 2002; 117(2):167–72. [PubMed: 12100982]
30. Chen D, et al. Effect of dimethyl sulfoxide on bladder tissue penetration of intravesical paclitaxel. Clin Cancer Res. 2003; 9(1):363–9. [PubMed: 12538489]
31. Smith KJ, Chess-Williams R, McDermott C. Luminal DMSO: effects on detrusor and urothelial/lamina propria function. Biomed Res Int. 2014; 2014:347616. [PubMed: 24949435]
32. Au, J.L-S.a.W. Guillaume. In: Lerner, M.S. Seth P.; Sternberg, Cora, editors. Intravesical chemotherapy of superficial bladder cancer: optimization and novel agents, in Textbook of Bladder Cancer. CRC Press; 2006.
33. La JH, Schwartz ES, Gebhart GF. Differences in the expression of transient receptor potential channel V1, transient receptor potential channel A1 and mechanosensitive two pore-domain K+ channels between the lumbar splanchnic and pelvic nerve innervations of mouse urinary bladder and colon. Neuroscience. 2011; 186:179–87. [PubMed: 21549810]
34. DeBerry JJ, Albers KA, Davis BM. Bladder hypersensitivity and transcriptional regulation of potassium channel subunit mRNA expression in mice with cystitis. J Pain. 2013; 14(4):S57.
35. Abd-Elsayed AA, et al. KCNQ channels in nociceptive cold-sensing trigeminal ganglion neurons as therapeutic targets for treating orofacial cold hyperalgesia. Mol Pain. 2015; 11:45. [PubMed: 26227020]
36. Hendrich J, et al. Electrophysiological correlates of hyperalgesic priming in vitro and in vivo. Pain. 2013; 154(10):2207–15. [PubMed: 23831864]
37. Aizawa N, et al. Inhibitory effects of retigabine, a Kv7 channel activator, on mechanosensitive primary bladder afferent activities and nociceptive behaviors in rats. Neurourol Urodyn. 2015
38. Steinlein OK. Genetic mechanisms that underlie epilepsy. Nat Rev Neurosci. 2004; 5(5):400–8. [PubMed: 15100722]
39. Chen X, Gebhart GF. Differential purinergic signaling in bladder sensory neurons of naive and bladder-inflamed mice. Pain. 2010; 148(3):462–72. [PubMed: 20045252]
40. Wilson SR, et al. The epithelial cell-derived atopic dermatitis cytokine TSLP activates neurons to induce itch. Cell. 2013; 155(2):285–95. [PubMed: 24094650]
41. Ikeda R, et al. Merkel cells transduce and encode tactile stimuli to drive Abeta- afferent impulses. Cell. 2014; 157(3):664–75. [PubMed: 24746027]
42. Baumbauer KM, et al. Keratinocytes can modulate and directly initiate nociceptive responses. Elife. 2015; 4
43. Janig W. Neurobiology of visceral afferent neurons: neuroanatomy, functions, organ regulations and sensations. Biol Psychol. 1996; 42(1-2):29–51. [PubMed: 8770369]
44. Cervero F, Connell LA, Lawson SN. Somatic and visceral primary afferents in the lower thoracic dorsal root ganglia of the cat. J Comp Neurol. 1984; 228(3):422–31. [PubMed: 6480920]
45. Grundy D. Signalling the state of the digestive tract. Auton Neurosci. 2006; 125(1-2.):76–80. [PubMed: 16473562]
46. Dang K, Bielefeldt K, Gebhart GF. Differential responses of bladder lumbosacral and thoracolumbar dorsal root ganglion neurons to purinergic agonists, protons, and capsaicin. J Neurosci. 2005; 25(15):3973–84. [PubMed: 15829649]
47. Gold MS, Shuster MJ, Levine JD. Characterization of six voltage-gated K+ currents in adult rat sensory neurons. J Neurophysiol. 1996; 75(6):2629–46. [PubMed: 8793767]

Highlights

- Two populations of pelvic nerve urinary bladder afferents were identified.
- DRG bladder neurons were labeled by intraparynchemal or intravesical dye administration.
- Urothelial and non-urothelial afferents exhibit intrinsic differences in excitability.

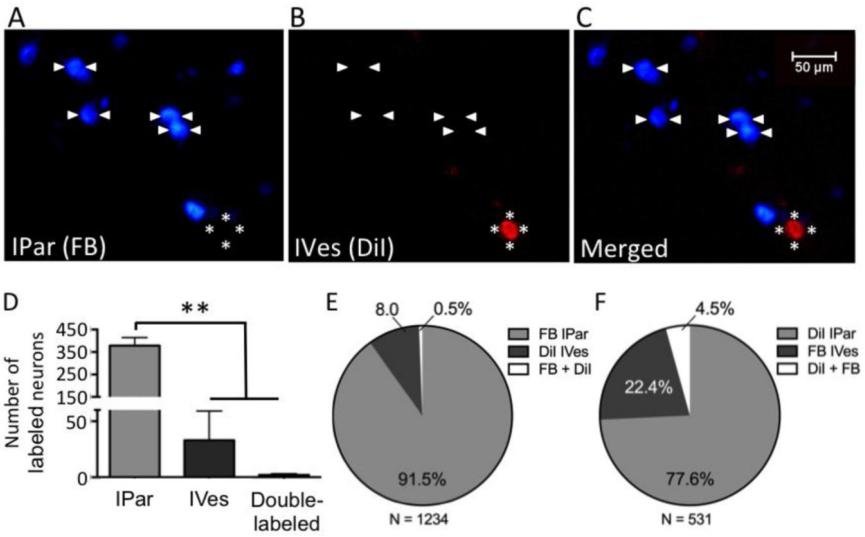

Figure 1. IPar- and IVes-labeled neurons are anatomically distinct subsets of PN bladder afferents

Intraparynchemal (IPar) injection of FB and intravesical (IVes) infusion of DiI retrogradely labeled two subpopulations of bladder-innervating L6 DRG neurons (**A-C**). Arrowheads indicate IPar neurons labeled by FB and asterisks indicate a DiI-positive, IVes neuron. One wk after dye administration, the total number of L6 DRG neurons labeled by IPar FB was significantly higher than the number labeled by IVes DiI or by both FB and DiI (**D**). Of a total of 1234 labeled L6 DRG neurons, 91.5% were positive for FB, 8% were positive for DiI, and 0.5% were double-labeled (**E**). When dyes were reversed, 77.6% of IPar-labeled neurons were positive for DiI, 22.4% IVes-labeled neurons were positive for FB, and 4.5% were double-labeled out of a total of 531 labeled neurons (**F**). ** indicates P<0.01.

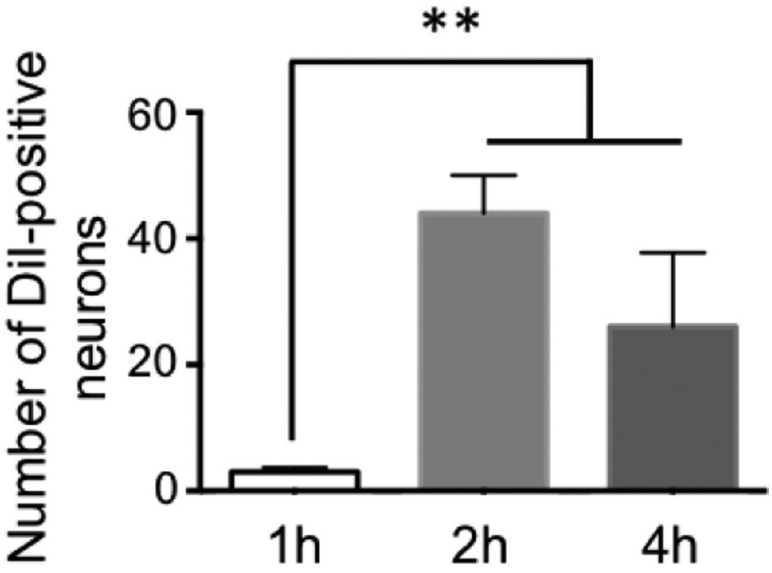

Figure 2. IVes labeling is time-dependent

A parametric study revealed that the number of neurons labeled by a 2 h or 4 h IVes infusion of DiI did not differ, but both 2 and 4 h labeled significantly more neurons than a 1 h dwell time. ** indicates P<0.01.

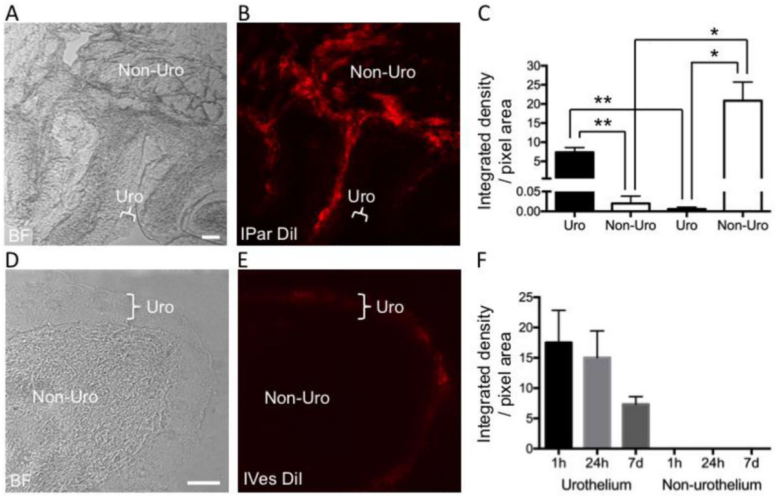

Figure 3. Fluorescent dye is differentially distributed in bladder tissue following IPar and IVes labeling

Technique-dependent patterns of DiI distribution within the bladder were observed following IPar DiI injection and IVes DiI infusion. As seen in (**A**) and (**C**), non-urothelial bladder tissue (indicated by Non-Uro) could be differentiated from the urothelium (indicated by Uro) using bright field (BF) microscopy at 10× and 20×, respectively. The distribution of DiI in the same tissue sections (**B, D**) was quantified by determining the integrated density in urothelial and non-urothelial regions. In IVes-labeled mice, urothelial labeling was significantly greater than non-urothelial labeling, and in IPar-labeled mice, the opposite was true (**C**). Further, urothelial labeling was greater in IVes- than in IPar-labeled tissue, and non-urothelial labeling was greater in IPar- versus IVes-labeled tissue. The distribution of DiI in the bladder following IVes labeling did not change over time (**F**). * indicates $P<0.05$, ** indicates $P<0.01$.

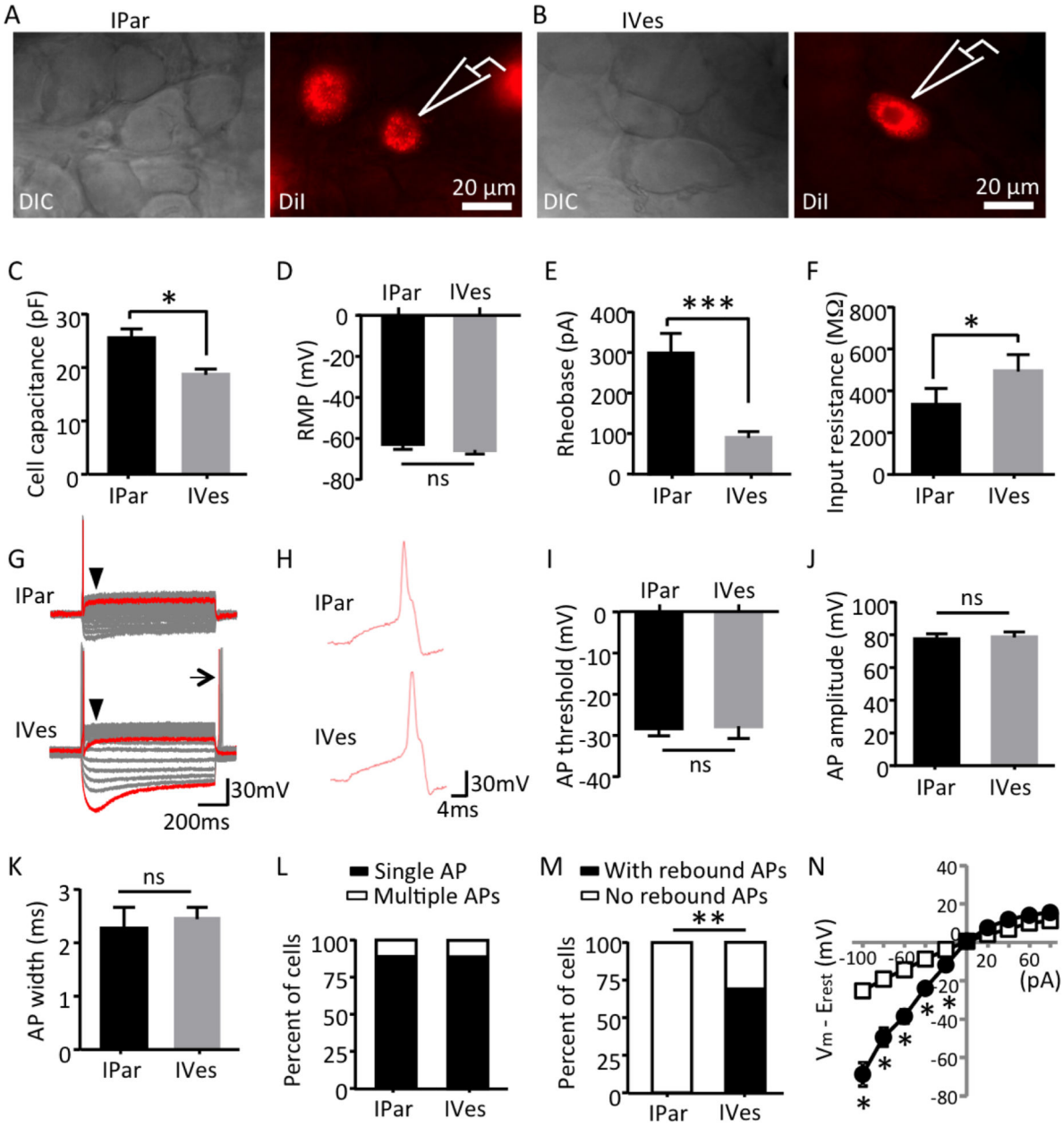

Figure 4. Urothelial and non-urothelial neurons exhibit different intrinsic electrophysiological properties

Differential interference contrast (DIC) and epifluorescence were used to identify DiI-positive PN bladder neurons that were retrogradely labeled by the IPar (**A**) or IVes (**B**) method. Passive and active characteristics were determined, and a comparison between neuron types revealed several differences, as shown by representative traces in (**C**). Both non-urothelial (IPar-labeled) and urothelial (IVes-labeled) neurons exhibited an inflected somal spike pattern in the repolarization phase (**D**). Resting membrane potential was similar between groups (**E**), but rheobase was significantly lower in urothelial than in non-urothelial neurons (**F**). AP threshold (**G**) and AP width (**H**) did not differ and 90% (9/10) of the neurons in each grouped fired single APs (**I**), as shown by the red traces in (**C**). Urothelial

neurons, however, were more likely to fire rebound APs than non-urothelial neurons (**J**), as indicated by the arrow in the lower panel of (**C**). Rebound APs may be a result of significantly higher hyperpolarization-activated “sag” potential in urothelial versus non-urothelial neurons (**K**), as shown by the blue traces in (**C**). Sag potential was measured as the difference in potentials between the black and white triangles (**C**). Finally, input resistance was lower (**L**) and cell capacitance higher (**M**) in non-urothelial neurons. N=10 neurons obtained from 3 animals/group. * indicates $P<0.05$; ** indicates $P<0.01$; *** indicates $P<0.001$.

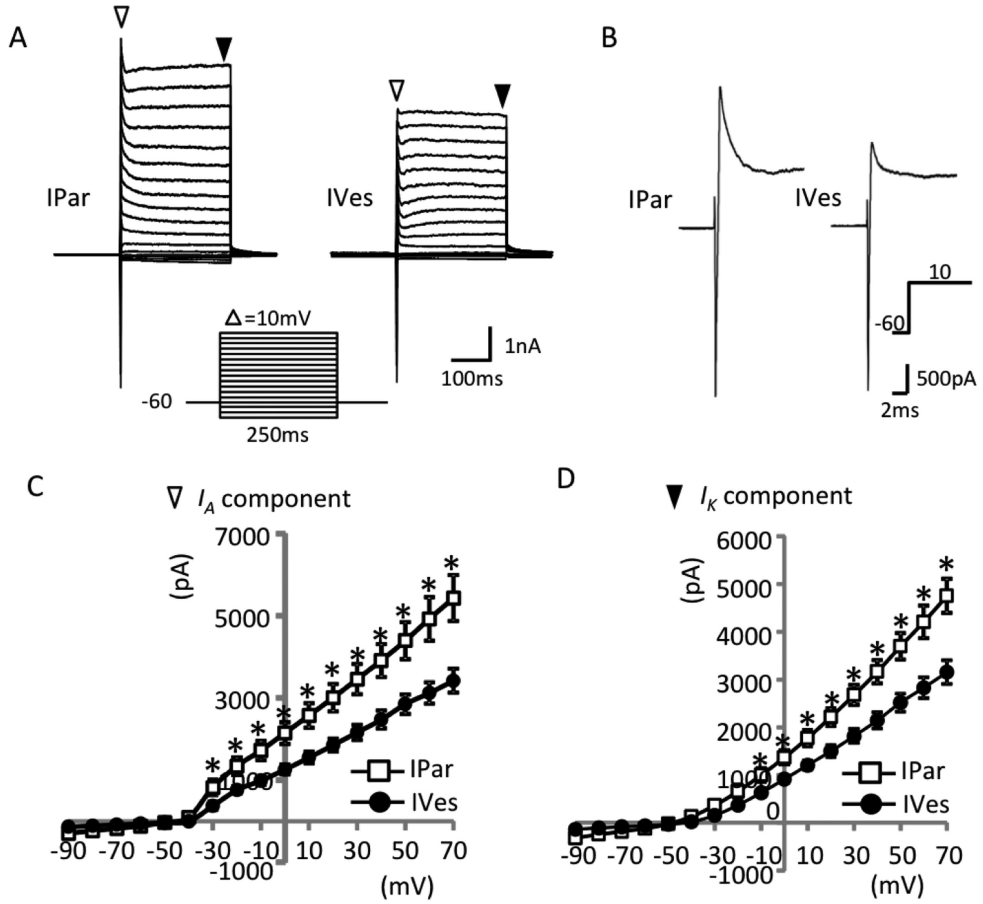

Figure 5. Magnitude of outward currents differs between urothelial and non-urothelial PN bladder neurons

Representative traces of total currents evoked by voltage steps (shown below the traces) from a holding potential of −73 mV revealed an inactivating inward current, an inactivating outward current (white triangles), and a non-inactivating outward current (black triangles) (**A**). The inactivating outward currents measured in non-urothelial (IPar-labeled) neurons were significantly higher at voltage steps ranging from −43 to +57 mV than in urothelial (IVes-labeled) neurons (**B,C**). Similarly, the non-inactivating outward current measured in non-urothelial relative to urothelial neurons was significantly higher at voltage steps of −23 to +57 mV (**D**). N=10 neurons obtained from 3 animals/group. * indicates P<0.05.

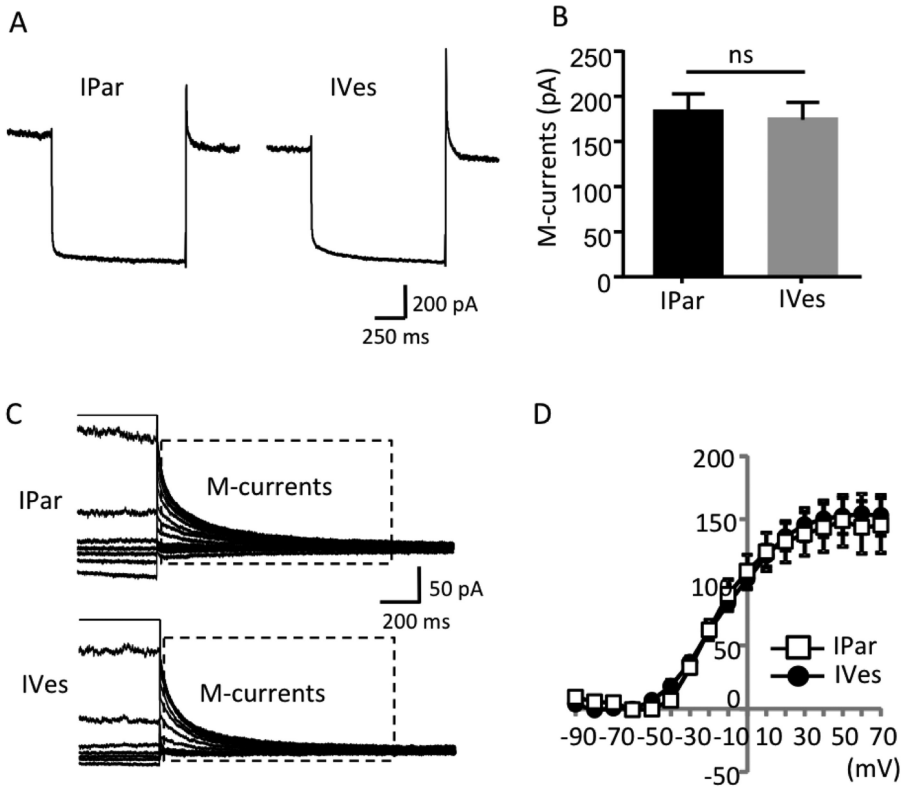

Figure 6. PN bladder neurons exhibit robust M-currents

Representative traces in response to a voltage step from −73 to +7 mV show similar magnitude of peak M-currents between non-urothelial (IPAR-labeled) and urothelial (IVes-labeled) neurons (**A**), and a quantitative comparison of peak M-currents showed no difference between groups (**B**). The box shown on the sample traces of M-currents obtained in response to a series of voltage steps ranging from −103 to +57 indicate the M-currents, measured by tail currents after each voltage step (**C**). *I*-V curves of tail currents from urothelial and non-urothelial bladder neurons did not differ in response to voltage steps ranging from −103 to +57 mV (**D**).